# Contributions of higher angular momentum states to lateral resolution in scanning tunneling microscopy

**Šestović, Dragan; Šunjić, Marijan**

# Contributions of higher angular momentum states to lateral resolution in scanning tunneling microscopy

Dragan Šestović and Marijan Šunjić
*Department of Physics, University of Zagreb, Bijenička cesta 32, 41000 Zagreb, Croatia*
(Received 3 November 1994)

We investigate the influence of higher angular momentum states (AMS's) to the formation of a scanning tunneling microscopy (STM) image. We calculate the tunneling current between the STM tip, represented by the rotational paraboloid, and the sample, consisting of hemispherical protrusions on the flat metallic surface, using the Bardeen transfer Hamiltonian method. The electron wave function in the paraboloidal tip is expanded in the AMS's which are the eigenstates of a spherical tip. The total STM image can be constructed using the matrix elements for the tunneling of these particular states. We numerically simulate the STM image of a sample surface and calculate the contributions of a particular AMS to the STM image and to the lateral resolution, showing that higher AMS's essentially improve the resolution in the STM image. Contributions and lateral resolutions of various angular momentum channels are found to depend strongly on the curvature on the tip apex.

## I. INTRODUCTION

Many papers in the past decade studied theoretical interpretation of scanning tunneling microscopy (STM) images and physical phenomena which occur when a sharp STM tip scans a sample surface.[1–7] Still there is no final answer to the basic question, what does a STM image represent? It is only obvious that the STM image is not a direct topographic map of ion positions on the surface but rather a function of the electron distribution in the tip-sample system.

In the present work we investigate the electron tunneling between a paraboloidal STM tip and hemispherical protrusions on the flat metallic surface (Fig. 1). We shall be especially concerned with the influence of the tip curvature and electronic states in the tip on the STM image. Hemispherical protrusions represent three-dimensional (3D) islands on the substrate surface which can be formed, e.g., by Volmer-Weber (3D islands) or Stranski-Krastanov (3D islands on one or few layers) modes of epitaxial growth.[8–10] We shall use the Bardeen transfer Hamiltonian method[2] (THM) for the calculation of the tunneling current, which enables us to treat the electronic states in the tip and in the sample separately.

This method was used first by Tersoff and Hamman,[2] who treated the tip electronic states approximately, assuming that the vacuum tail of the tip wave function can be represented by the vacuum part of the spherically symmetric $s$ state, i.e., the lowest angular momentum state (AMS) of the spherical potential well. Such an approximation led them to the conclusion that the tunneling current between the tip and the sample is proportional to the local electronic density of states (LDOS) of the sample at the Fermi level, but the predicted resolution was in disagreement with the experimentally achieved resolution.[11–13] One way to resolve the contradiction between the experiment and theory is the inclusion of the higher AMS in the simulation of the STM image, and several authors have approached the problem in this way. Chung *et al.*[14] studied discrete bound states in a spherical tip model of the potential. They found that contribution of the $p$ state should be taken into account and that this contribution improves the resolution in the STM image. Detailed theory of the derivation of the tunneling matrix elements by expanding the vacuum tail of the tip and sample wave functions in terms of complete sets of AMS's and eigenfunctions in parabolic coordinates was developed by Chen.[15,16] The total tunneling matrix element was connected with the coefficients in the expansions in a simple way. Chen also suggested[17] the importance of the higher AMS, especially the contribution of the $d_{z^2}$ state on a tungsten tip to the atomic resolution in STM.

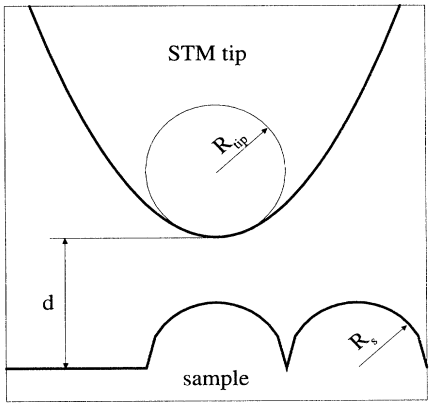


FIG. 1. Paraboloidal STM tip scans the sample, which is represented by hemispherical protrusions on a flat metallic surface.

 

Improvement of the resolution in STM from the $p$ component of the tip wave function was shown by Lawunmi and Payne.[18]

In this paper we present results of a model where the STM tip is represented by the rotational paraboloid. The electronic wave function of the electron in such a tip, which can be determined exactly only in the infinite barrier model (IBM), is projected on the AMS. A sample is represented by the flat metallic surface with one or two hemispherical protrusions. The electron wave function in such a sample is calculated numerically by the finite difference method (FDM). We separately investigate tunneling of different AMS's through the potential barrier and the total tunneling current. In this way we decompose the resulting STM image into contributions of particular AMS's, i.e., images of various angular momentum channels. The total current is obtained by the summation of all angular momentum contributions and the mixing terms between channels.

Our results suggest that the higher AMS, even higher than the $d$ state, cannot be ignored in the theoretical considerations, especially for greater curvatures at the tip apex. Besides, higher AMS's contribute to the better resolution in the STM images.

In Sec. II we briefly present the basic tunneling formalism used in this paper. In Sec. III we use the paraboloidal tip model as a useful geometric model of the STM tip and decompose the wave function of the paraboloid in the AMS. Results of theoretical simulations of the STM images with a discussion are presented in Sec. IV. A brief sketch of the FDM used in our problem is presented in the Appendix.

## II. FORMALISM

Using Bardeen's transfer Hamiltonian method we can calculate the tunneling current between the tip and the surface at low temperature and in the low bias limit from the following expression:[19]

$$I = \frac{2\pi}{\hbar} e^2 V \sum_{t,s} |M_{t,s}|^2 \delta(E_t - E_F)\delta(E_s - E_F), \qquad (1)$$

where $M_{t,s}$ is the matrix element for the transition from tip state $t$ to surface state $s$, given by

$$M_{t,s} = \frac{\hbar^2}{2m} \int d\mathbf{S}_{\mathrm{vac}} (\Psi_s^*, \nabla\Psi_t - \Psi_t \nabla\Psi_s^*), \qquad (2)$$

where $\Psi_t$ and $\Psi_s$ are the tip and sample wave functions, determined assuming infinitely separated electrodes. Integration can be obtained along any surface in the vacuum which separates the tip and the sample regions. In this way the whole problem is reduced to the calculation of the functions $\Psi_t$ and $\Psi_s$.

## III. PARABOLOIDAL MODEL OF THE STM TIP

It is a reasonable assumption to represent the tip shape by a rotational paraboloid (Fig. 1). We can exactly determine the electron states of the paraboloidal tip in the IBM by solving the Schrödinger equation in the paraboloidal coordinate system.[20] We define paraboloidal variables $\xi$, $\eta$, and $\varphi$, where $\xi$ and $\eta$ represent two families of rotational paraboloids, one with the opening in the positive $z$ direction and the other in the negative direction, and $\varphi$ is the angle of rotation (Fig. 2). The relations of variables of the rectangular $(x, y, z)$ and the spherical $(\rho, \theta, \varphi)$ system are given by

$$x = \cos\varphi\sqrt{\xi\eta}, \qquad (3a)$$

$$y = \sin\varphi\sqrt{\xi\eta}, \qquad (3b)$$

$$z = \frac{\eta - \xi}{2}, \qquad (3c)$$

$$\varphi = \varphi, \qquad (3d)$$

$$\xi = r(1 - \cos\theta), \qquad (3e)$$

$$\eta = r(1 + \cos\theta), \qquad (3f)$$

$$\xi, \eta \geq 0. \qquad (3g)$$

The paraboloidal coordinate system is obviously convenient because one coordinate surface ($\xi = \xi_0$) coincides with the surface of the tip, as defined by

$$z = \frac{x^2 + y^2 - \xi_0^2}{2\xi_0}. \qquad (4)$$

The variable $\xi_0$ is equal to the radius of curvature of the

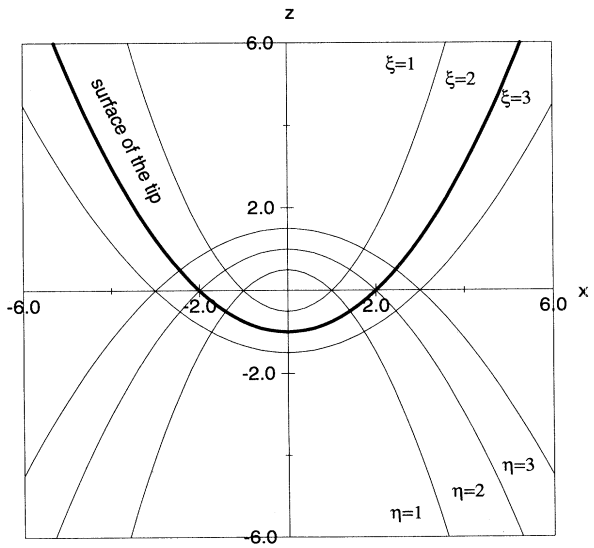


FIG. 2. The shape of the $\xi$ and $\eta$ coordinate surfaces on the $x$-$z$ section plane. The bold curve represents the surface of the tip.

paraboloid at its apex.

Potential in the IBM is given by

$$V(\xi,\eta,\varphi)=\begin{cases}0 & \text{if } \xi\le\xi_0\\ \infty & \text{if } \xi>\xi_0.\end{cases} \tag{5}$$

The Schrödinger equation for the electron in the tip is

$$\frac{4}{\eta+\xi}\left[\frac{\partial}{\partial\xi}\left(\xi\frac{\partial\Psi}{\partial\xi}\right)+\frac{\partial}{\partial\eta}\left(\eta\frac{\partial\Psi}{\partial\eta}\right)\right]+\frac{1}{\xi\eta}\frac{\partial^2\Psi}{\partial\varphi^2}+k^2\Psi=0, \tag{6}$$

where $k$ is

$$k^2=\frac{2mE}{\hbar^2}. \tag{7}$$

Writing the solution in the form

$$\Psi(\xi,\eta,\varphi)=f(\xi)g(\eta)h(\varphi), \tag{8}$$

we get three equations for the functions $f(\xi)$, $g(\eta)$, and $h(\varphi)$:

$$\frac{d}{d\xi}\left(\xi\frac{df}{d\xi}\right)+\left(\frac{k^2\xi}{4}-\frac{m^2}{4\xi}-\nu\right)f=0, \tag{9}$$

$$\frac{d}{d\eta}\left(\eta\frac{dg}{d\eta}\right)+\left(\frac{k^2\eta}{4}-\frac{m^2}{4\eta}+\nu\right)g=0, \tag{10}$$

$$\frac{d^2h}{d\varphi^2}=-m^2h. \tag{11}$$

The solutions are

$$h_m(\varphi)=\frac{e^{\pm im\varphi}}{\sqrt{2\pi}}, \tag{12}$$

$$f_{m,\nu}(k,\xi)=A\xi^{-1/2}M_{i\frac{\nu}{k};\frac{|m|}{2}}(ik\xi), \tag{13}$$

$$g_{m,\nu}(k,\eta)=B\eta^{-1/2}M_{-i\frac{\nu}{k};\frac{|m|}{2}}(ik\eta), \tag{14}$$

where $\nu$ is the separation constant and $M_{\lambda,\mu}$ is the Whittaker function.[20,21] The boundary condition for the wave function in the IBM,

$$f_{m,\nu}(k,\xi_0)=0, \tag{15}$$

implies that for fixed $k$, i.e., electron energy, and azimuthal quantum number $m$ there is a discrete spectrum of possible values of the separation constant $\nu$ defining the new integer quantum number $n$. The electronic state in the rotational paraboloid is therefore determined by the three quantum numbers $k$, $m$, and $n$, and the wave function is

$$\Psi_{n,m}(k,\vec{r})=\frac{e^{\pm im\varphi}}{\sqrt{2\pi}}f_{n,m}(k,\xi)g_{n,m}(k,\eta). \tag{16}$$

Results of the numerical calculation of possible electron energies for various values of the separation constant $\nu$ are shown in Fig. 3. The meaning of the quantum number $n$ is more obvious in Fig. 4, where we present the wave function $f_{n,m}(k,\xi)$ along the coordinate $\xi$: $n$ determines the number of nodes of the wave function.

For the calculation of the tunneling current in the THM we must know the tail of the tip electronic wave function in the vacuum, so we should determine the wave function in the finite potential. This cannot be done analytically by separating the variables, because the potential in that case depends on the coordinate $\xi$ and enters in both differential equations for $f(\xi)$ and for $g(\eta)$ through the wave vector $k(\xi)^2=2m[E-V(\xi)]/\hbar^2$. Therefore we have to use an approximative approach. First, we shall decompose the stationary state wave function of the rotational paraboloid (16), obtained in the IBM, in the AMS, i.e., the free electron wave functions in the spherical coordinate system:

$$\Psi^{\rm in}_{n,m}(k,\vec{r})=\sum_{l,m'}C^{l,m'}_{n,m}(k)\phi^{\rm in}_{l,m'}(k,\vec{r}), \tag{17}$$

where

$$\phi^{\rm in}_{l,m}(k,\vec{r})=j_l(kr)Y^m_l(\theta,\varphi) \tag{18}$$

and $k$ is given by (7). Coefficients in the series (17) can be calculated from

$$C^{l,m'}_{n,m}(k)=\int_{\rm in}dV[\phi^{\rm in}_{l,m'}(k,\vec{r})^*\Psi^{\rm in}_{n,m}(k,\vec{r})], \tag{19}$$

where integration is made inside the tip region. The volume element in the paraboloidal system is[20]

$$dV=\frac{\eta+\xi}{4}d\xi d\eta d\varphi, \tag{20}$$

which leads to the final expression:

$$C^{l,m'}_{n,m}(k)=\delta_{m,m'}\int_0^\infty d\eta\times\int_0^{\xi_0}d\xi\frac{\eta+\xi}{4}f_{n,m}(k,\xi)g_{n,m}(k,\eta)\times\sqrt{\frac{2l+1}{2}\frac{(l-m')!}{(l+m')!}}P^{m'}_l(\cos(\theta))j_l(kr). \tag{21}$$

If we now introduce the finite potential step $V_0$ on the tip surface, tip states will be allowed to extend in the barrier region. We can match the state in the tip $\phi^{\rm in}_{l,m'}$ (18) with the vacuum part of the AMS, which is given for $E<V_0$ by

$$\phi^{\rm vac}_{l,m}(\kappa,\vec{r})=\frac{j_l(kR)}{h^{(1)}_l(i\kappa R)}Y^m_l(\theta,\varphi)h^{(1)}_l(i\kappa r), \tag{22}$$

where $\kappa$ is given by

$$\kappa=\sqrt{\frac{2m(V_0-E)}{\hbar^2}}. \tag{23}$$

Therefore we represent the vacuum part of the tip wave

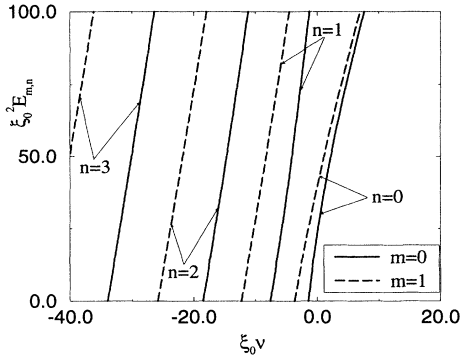


FIG. 3. Electron energy versus the separation constant $\nu$ for $m = 0, 1$ and $n = 0, 1, 2, 3$.

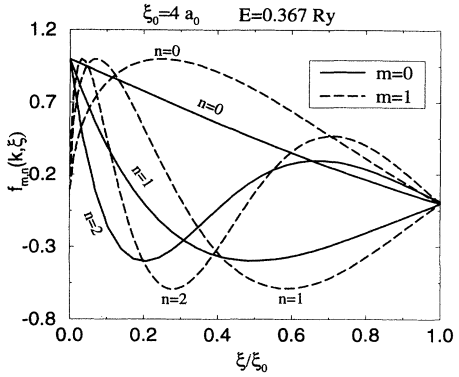


FIG. 4. Wave functions $f_{m,n}(E,\xi)$ for $m = 0, 1$, $E = 0.367$ Ry, and $n = 0, 1, 2$.

function by the relation

$$\Psi^{\rm vac}_{n,m}(k,\vec{r}) = \sum_l C^{l,m}_{n,m}(k)\phi^{\rm vac}_{l,m}(\kappa,\vec{r}), \tag{24}$$

where $C^{l,m}_{n,m}(k)$ is calculated approximately by (21). We can make such an approximation because the area active in the tunneling process is a narrow region near the tip apex where the surface of the paraboloidal tip and a sphere with radius $R_{\rm tip} = \xi_0$ coincide (Fig. 1).

Now we can calculate the matrix elements for the tunneling and total tunneling current from (1), (2), (21), and (24). The matrix element for the tunneling from the tip state $t$ to the state $s$ in the sample is then given by

$$M_{t\to s} = \sum_g C^g_t M_{g\to s}, \tag{25}$$

where $g$ is the abbreviation for the quantum numbers of the AMS $(l, m, \kappa)$ and $M_{g\to s}$ is the matrix element for the tunneling from the AMS in the tip to the surface state $s$:

$$M_{g\to s} = -\frac{\hbar^2}{2m}\int d\mathbf{S}[(\phi_{l,m}(\kappa,\vec{r}))^*\nabla\Psi_s - \Psi_s\nabla(\phi_{l,m}(\kappa,\vec{r}))^*]. \tag{26}$$

The total conductivity in the system is

$$\sigma = \frac{2\pi e^2}{\hbar}\sum_t\sum_g\sum_s |C^g_t|^2|M_{g\to s}|^2\delta(E_g - E_F)\delta(E_s - E_F) + \frac{2\pi e^2}{\hbar}\sum_t\sum_{g\neq g'}\sum_s \frac{1}{2}{\rm Re}\left[(C^g_t)^* C^{g'}_t M_{g\to s}(M_{g'\to s})^*\right]\delta(E_g - E_F)\delta(E_{g'} - E_F)\delta(E_s - E_F). \tag{27}$$

The first term in this expression represents the direct contributions of different angular momentum channels and the second term represents the mixing terms between channels.

## IV. RESULTS AND DISCUSSION

In this section we present results of the theoretical simulation of the STM image in the case where the paraboloidal tip scans, at constant height, the sample which consists of one or two hemispherical protrusions on a flat metallic surface (see Fig. 1). This enables us to analyze the contributions of a particular AMS to the total tunneling current and therefore to the STM image. The stationary state electron wave function in the sample is calculated numerically by the FDM as described in the Appendix.

We assume that the tip is the rotational paraboloid with a radius of curvature $R_{\rm tip} = 4$ a.u. at the tip apex. This surface coincides with coordinate surface $\xi_0 = R_{\rm tip}$ in the paraboloidal coordinate system. The wave function of the tip is given by (16). Among possible tip states we select the state determined by quantum numbers $E = 5$ eV (typical metallic work function) and for the sake of simplicity $n = 0$ (one node along $\xi$ inside the tip) and $m = 0$. Following the arguments of Lucas *et al.*,[6] we neglect the contributions of the states with $m \neq 0$ in our considerations. The vacuum part of the electron wave function in the tip is expanded in the AMS (24), where the weight factors for particular components are calculated from (21).

In the first case we assume one hemispherical protrusion with radius 4 a.u. positioned on the flat metallic surface, which is scanned with a paraboloidal tip at the distance 6 a.u. between the tip apex and the flat surface. We calculated the matrix elements for the transitions of the particular momentum states between the tip and the sample by Eq. (2) and total conductivity by (27). The STM image is formed by the values of the conductivities ($z$ axis) for particular positions of the tip above the

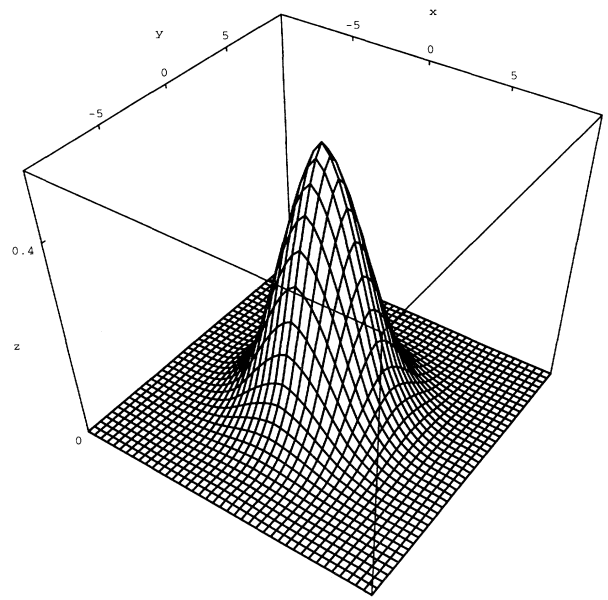


FIG. 5. STM image of the sample with one hemispherical protrusion (with $R_s = 4$ a.u.). The image is formed by the calculated values of the conductivities in $10^{-9}\ \Omega^{-1}$ ($z$ axis). The paraboloidal tip ($\xi_0 = 4$ a.u.) scans the sample at the height 6 a.u.

sample ($x$ and $y$ axes), and is shown in Fig. 5.

In the second case we assume two equal hemispherical protrusions with radii 4 a.u. which touch each other on the flat surface (Fig. 1). We repeat the previous procedure and calculate the STM image of this sample. The result of the calculation is shown in Fig. 6. One can see

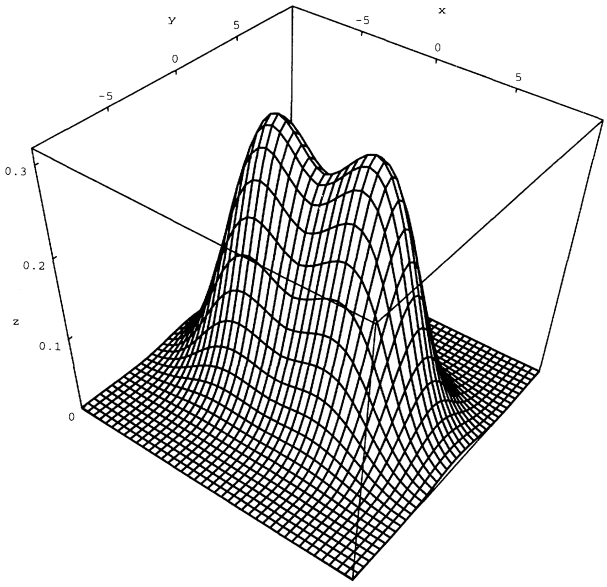


FIG. 6. STM image of the sample with two hemispherical protrusions (with $R_s = 4$ a.u.). The image is formed by the calculated values of the conductivities in $10^{-9}\ \Omega^{-1}$ ($z$ axis). The paraboloidal tip ($\xi_0 = 4$ a.u.) scans sample at the height 6 a.u.

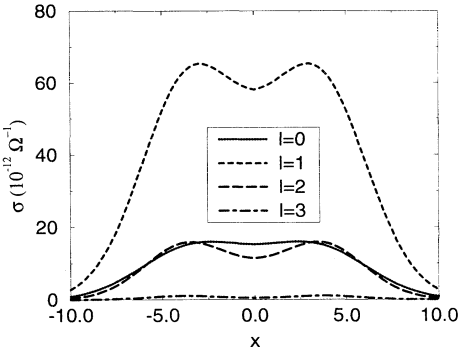


FIG. 7. Decomposition of the STM image in Fig. 6 (along the $x$ axis) into images from $l = 0, 1, 2, 3$ momentum channels, along the $x$ axis.

one great protrusion with two visible maxima above the centers of the hemispheres. Contributions of particular angular momentum channels to the total image are investigated, defining the intensity of a particular channel as the contribution to the total conductivity from the transitions between the tip state $(l, m = 0)$ and the sample state $s$ by

$$\sigma_l = \frac{2\pi}{\hbar} e^2 |M_{l\to\nu}|^2 \delta(E_l - E_F)\delta(E_\nu - E_F). \qquad (28)$$

In such a manner we calculated the intensities of particular channels when the tip moves above the line passing through the centers of hemispherical protrusions, as shown in Fig. 7. We can see that only three lower angular momentum channels $l = 0, 1, 2$ give essential contributions to the total image in this case, and the $l = 1$ channel has the highest intensity. It is interesting that the $l = 0$ channel contribution cannot resolve the two protrusions, and only for high channels are the protrusions well separated. This leads us to the obvious conclusion that higher AMS's contribute to the better resolution in STM, due to the fact that $m = 0$ angular momentum states (investigated here) with higher $l$ are mostly directed along the $z$ axis, and become sharper with $l$.

From this study we can also determine the influence of the radius of curvature of the tip apex, i.e., the sharpness

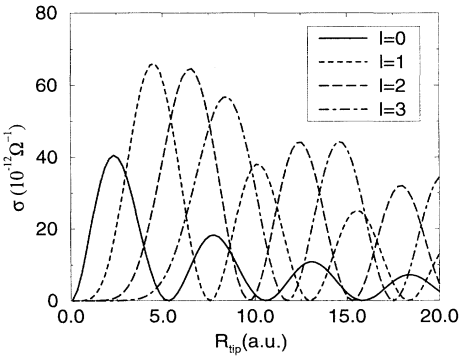


FIG. 8. Dependence of $\sigma_l$ (28) on the radius of curvature at the tip apex $R_{\rm tip}$, when the tip is positioned above the center of one protrusion.

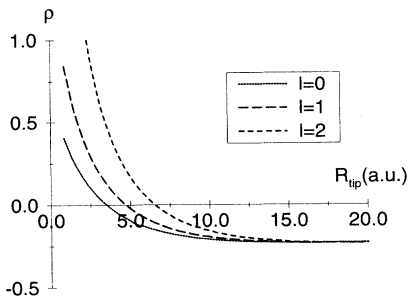


FIG. 9. Dependence of the resolution $\rho$ of the $l = 0, 1, 2$ momentum channels on the radius of curvature ($R_{\rm tip}$) on the tip apex.

of the tip, on the role of different channels in STM. Let us fix the tip position above the center of one hemispherical protrusion and change the radius of the curvature ($R_{\rm tip}$) of the tip apex but without changing the distance between the tip and the sample (Fig. 1). We calculated the conductivities in this system for different radii of curvatures and for the different channels, as shown in Fig. 8 for $l = 0, 1, 2, 3$ channels. The intensities of all channels oscillate with the tip radius. For a very sharp tip ($R_{\rm tip} < 2$ a.u.) the channel $l = 0$ is dominant, due to the fact that higher AMS's cannot exist near the tip apex which is the relevant region for tunneling, but this channel loses importance for greater $R_{\rm tip}$. For the tip with $R_{\rm tip} = 4$ a.u. the $l = 1$ channel dominates but $l = 0$ and 2 channels also make appreciable contributions. Channel $l = 3$ appears at $R_{\rm tip} \approx 6$ a.u. and dominates for $R_{\rm tip} \approx 8$ a.u.

We can define the lateral resolution of the hemispherical defects in STM image as

$$\rho = \frac{\sigma_{\rm center} - \sigma_{\rm middle}}{\sigma_{\rm middle}}, \tag{29}$$

where $\sigma_{\rm center}$ is the conductivity for the tip above the protrusion center and $\sigma_{\rm middle}$ is the conductivity for the tip above the middle point between the two hemispheres. We study the influence of $R_{\rm tip}$ on the resolution of particular angular momentum channels. The results for the $l = 0, 1, 2$ channels are shown in Fig. 9 and it is evident that higher channels have better resolution, but there is a critical value of $R_{\rm tip}$ for which $\rho$ changes sign, which means that the two protrusions become unresolvable in the STM image.

## V. CONCLUSIONS

We have extended the Tersoff and Hamman theory of STM by including higher angular momentum states with the help of the geometric model of STM tip based on its representation by the rotational paraboloid. The vacuum tail of the tip wave function has been expanded in the AMS, as in the earlier work by Chen[15–17] and the coefficients in the expansion have been numerically calculated. We have applied this model to a sample that consists of a flat metallic surface with one or two hemispherical protrusions. Although the tunneling matrix elements for particular AMS (in the tip and the surface), up to $l = 2$, were already derived in simple analytical form,[16] we have calculated them numerically for all $l$ and for a simulated surface. In this way we have decomposed the STM image into various angular momentum channels and systematically analyzed their intensities and resolutions. Numerical simulations demonstrated that (i) higher AMS's should be taken into account, especially for the radius of curvature at the tip apex ($R_{\rm tip}$) greater than 2 a.u.; (ii) the contributions of particular momentum channels to STM are greatly influenced by $R_{\rm tip}$; (iii) higher momentum channels essentially contribute to the better resolution in STM; and (iv) the resolution of the image formed by particular channels decreases with the the tip radius, but much more slowly for higher angular momentum channels.

## APPENDIX: DETERMINATION OF THE SAMPLE STATES

Determination of electronic states in metallic solids of arbitrary shapes analytically, by direct integration of the Schrödinger equation using the separation of variables method, is possible only for a few cases. The condition which must be satisfied is that the surface of the solid must coincide with the coordinate surface of some coordinate system in which the Schrödinger equation is separable.[20] For a general shape the determination of wave functions is possible only numerically. For such a calculation we can use the finite difference method. Our equation is

$$\triangle\Psi(x,y,z) + k(x,y,z)^2\Psi(x,y,z) = 0, \tag{A1}$$

where finite barrier $V_0$:

$$k(x,y,z)^2 = \begin{cases} E & \text{in the metal} \\ E - V_0 & \text{in the vacuum.} \end{cases} \tag{A2}$$

We can choose any shape of the body. In Sec. IV this method is used for hemispherical protrusions on the flat metallic surface.

We impose the boundary conditions on the faces on the large cube: ($x_{a,b} = \pm L/2$, $y_{a,b} = \pm L/2$, $z_{a,b} = \pm L/2$),

$$\Psi(\pm L/2, \pm L/2, \pm L/2) = 0. \tag{A3}$$

After discretization the initial differential equation by the construction of the three-dimensional net

$$x_i = x_a + (i-1)d_x,$$
$$i = 1, 2, ..., n_x,$$
$$d_x = \frac{x_b - x_a}{n_x - 1}, \tag{A4}$$

we get an equation of differences,

$$\Psi(i,j,k-1)+\Psi(i,j-1,k)+\Psi(i-1,j,k)+\left\{\left[E-V(i,j,k)\right]d^2-6\right\}\Psi(i,j,k) + \Psi(i+1,j,k)+\Psi(i,j+1,k)+\Psi(i,j,k+1)=0. \quad \text{(A5)}$$

We can transform the tensors $\Psi(i,j,k)$ and $V(i,j,k)$ to vectors $\Psi(n)$ and $V(n)$ by transformation of indices

$$n=(k-1)n_x n_y+(i-1)n_y+j, \quad \text{(A6)}$$

where $n_x$, $n_y$, and $n_z$ are the numbers of nodes of the coordinate net in the $x$, $y$, and $z$ directions. This transformation leads to the equation

$$-\Psi(n-n_x n_y)-\Psi(n-n_y)-\Psi(n-1)+\left[V(n)d^2+6\right]\Psi(n)-\cdots \cdots-\Psi(n+1)-\Psi(n+n_y)-\Psi(n+n_x n_y)=Ed^2\Psi(n), \quad \text{(A7)}$$

which can be written in the matrix form

$$\widehat{A}\Psi=\lambda\Psi, \quad \text{(A8)}$$

where

$$\lambda=Ed^2. \quad \text{(A9)}$$

Matrix $\widehat{A}$ is a sparse matrix and all elements apart from those on the main diagonal $(n,n)$, neighboring diagonals $(n,n+1)$, $(n,n-1)$, and diagonals $(n,n+n_x n_y)$ $(n,n-n_x n_y)$ $(n,n+n_y)$ $(n,n-n_y)$ are zero. Certainly, all elements in these diagonals at the boundary (A3) are also equal to zero. The matrix eigenvalue problem (A8) can be solved by standard numerical routines.


[1] N. Garcia, C. Ocal, and F. Flores, Phys. Rev. Lett. **50**, 2002 (1983).
[2] J. Tersoff and D. R. Hamann, Phys. Rev. B **31**, 805 (1985).
[3] N. D. Lang, Phys. Rev. Lett. **55**, 230 (1985).
[4] N. D. Lang, Phys. Rev. Lett. **56**, 1164 (1986).
[5] Balaram Das and J. Mahanty, Phys. Rev. B **36**, 898 (1987).
[6] A. A. Lucas, H. Morawitz, G. R. Henry, J. P. Vigneron, Ph. Lambin, P. H. Cutler, and T. E. Feuchtwang, Phys. Rev. B **37**, 10 708 (1988).
[7] Th. Laloyaux, I. Derycke, J.-P. Vigneron, Ph. Lambin, and A. A. Lucas, Phys. Rev. B **47**, 7508 (1993).
[8] D. D. Chambliss, R. J. Wilson, and S. Chiang, Phys. Rev. Lett. **66**, 1721 (1991).
[9] S. Rousset, S. Chiang, D. E. Fowler, and D. D. Chambliss, Phys. Rev. Lett. **69**, 3200 (1992).
[10] H. Röder, R. Schuster, H. Brune, and K. Kern, Phys. Rev. Lett. **71**, 2086 (1993).
[11] V. M. Hallmark, S. Chiang, J. F. Rabolt, J. D. Swalen, and R. J. Wilson, Phys. Rev. Lett. **59**, 2879 (1987).
[12] Ch. Wöll, S. Chiang, R. J. Wilson, and P. H. Lippel, Phys. Rev. B **39**, 7988 (1989).
[13] J. Wintterlin, J. Wiechers, H. Burne, T. Gritsch, H. Höfer, and R. J. Behm, Phys. Rev. Lett. **62**, 59 (1989).
[14] M. S. Chung, T. E. Feuchtwang, and P. H. Cutler, Surf. Sci. **187**, 559 (1987).
[15] C. J. Chen, J. Vac. Sci. Technol. A **6**, 319 (1988).
[16] C. J. Chen, Phys. Rev. B **42**, 8841 (1990).
[17] C. J. Chen, Phys. Rev. Lett. **65**, 448 (1990).
[18] D. Lawunmi and M. A. Payne, J. Phys. Condens. Matter **2**, 3811 (1990).
[19] C. B. Duke, in *Tunneling in Solids*, edited by F. Seitz and D. Turnbull (Academic Press, New York, 1969).
[20] P. M. Morse and H. Feshbach, *Methods of Theoretical Physics* (McGraw-Hill, New York, 1953).
[21] J. S. Gradshteyn and J. M. Ryzhik, *Table of Integrals, Series and Products* (Academic, New York, 1965).